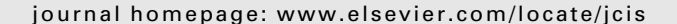
ELSEVIER

Contents lists available at ScienceDirect

Journal of Colloid and Interface Science





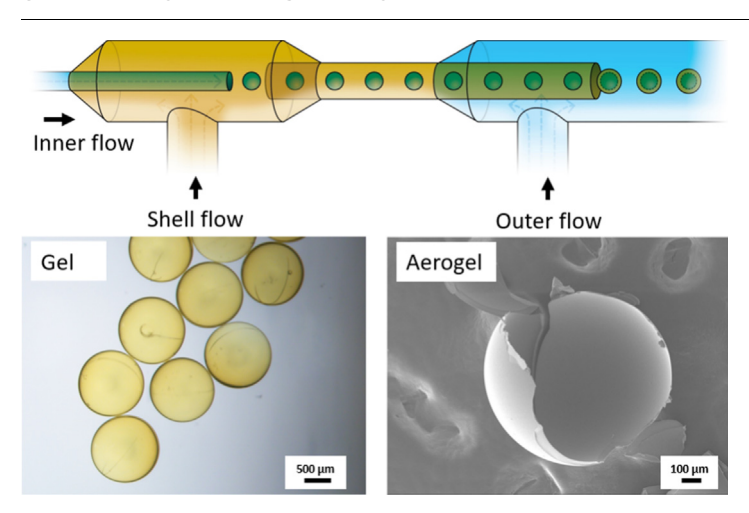
Continuous fabrication of core-shell aerogel microparticles using microfluidic flows



Nicholas Teo, Chenxi Jin, Akshata Kulkarni, Sadhan C. Jana*

Department of Polymer Engineering, The University of Akron, 250 South Forge Street, Akron, OH 44325-0301, United States

G R A P H I C A L A B S T R A C T



ARTICLE INFO

Article history: Received 22 October 2019 Revised 12 November 2019 Accepted 14 November 2019 Available online 15 November 2019

Keywords:
Aerogels
Polyimide
Core-shell
Microfluidics
Double emulsion

ABSTRACT

This work focuses on fabrication of core-shell polyimide aerogel microparticles with and without a surfactant via oil-in-oil-in-oil (O/O/O) emulsion system aided by a simple microfluidic device. A double emulsion is formed through sequential, step-wise emulsification of co-flowing core and shell organic liquid streams in a simple microfluidic setup. The polyimide sol, introduced as the shell liquid, undergoes accelerated polymerization in a heated silicone oil bath to yield a porous polyimide shell around silicone oil core that eliminates the possibility of droplet coalescence or rupture. The core-shell gel microparticles are then isolated and supercritically dried to obtain core-shell aerogel microparticles. The diameter and shell thickness of hollow microparticles are studied as function of liquid flowrates in the microfluidic device and the viscosity of the shell liquid.

© 2019 Elsevier Inc. All rights reserved.

1. Introduction

Microencapsulation is the process of shielding an internal dispersed phase from an external medium. This is usually achieved

through formation of a barrier or a coating layer that is either solid or is composed of an immiscible liquid phase. Microencapsulation technique has seen successful applications in industries such as food [1,2], cosmetics [3,4], fragrances [5], and pharmaceuticals [6]. Microencapsulation is often used as a means of containment, e.g., to mask odors, to hinder oxidation of encapsulated materials by creating diffusion barriers, and as a means of drug delivery

^{*} Corresponding author. E-mail address: janas@uakron.edu (S.C. Jana).

[7]. Microencapsulation is achieved using multiple techniques. These include spray drying [8], interfacial polymerization of polymer shells, and complex coacervation [9,10].

Emulsions are also useful in development of microencapsulation techniques. For example, Chu et al. [11] used the Shirasu porous glass (SPG) membrane emulsification process [12,13] to generate core-shell microcapsules. This was achieved by first generating oil-in-water (O/W) single emulsions through a glass membrane, followed by polymerization of the monomers at the O/W interface to obtain a hard shell, thereby encapsulating the oil phase and any materials incorporated in the oil phase. A number of microencapsulation techniques are also dependent on double emulsions. A double emulsion contains an emulsion inside an emulsion and was first described by Seifriz in 1925 [14]. Florence and Whitehill [15] categorized double emulsions into different types. In describing water-in-oil-in-water (W/O/W) double emulsions. Florence and Whitehill [15] identified type A double emulsions as drops containing only one internal droplet, type B as one with multiple internal droplets, and type C as globules entrapping large number of internal droplets. As is apparent, double emulsions exhibit additional instability events in comparison to single emulsions. These include coalescence of inner droplets inside the primary globules and coalescence of inner droplets at the globule interface [16]. In this context, a majority of research work on double emulsions focused on streamlining double emulsion formation process and improving double emulsion stability.

Conventionally, double emulsions are formed through a two-step emulsification process. The first step typically involves forming a W/O emulsion through high shear mechanisms such as sonication. This is followed by a second step where the initial W/O emulsion is incorporated into a separate water phase at significantly smaller shear rates to stabilize the first emulsion [17]. This method typically produces double emulsions that are polydisperse in diameter distribution, with diameter of a few tens of micrometer. Various parameters such as dispersed phase content, shear rate, and viscosity of the phases all influence diameter distribution in double emulsions [18]. Another important consideration is the formulation of appropriate surfactant package, e.g., surfactant types and loading levels [19,20]. In W/O/W double emulsions, a lipophilic surfactant is used in the shell organic liquid, while a hydrophilic surfactant is added to the exterior aqueous phase.

Double emulsions were also fashioned from microfluidic processes [21]. The main advantage of microfluidic droplet generation process is its high reproducibility and precise size control [22,23]. Monodisperse double emulsions are achieved through careful control of flow and shear conditions [24]. Monodisperse droplets are particularly attractive for drug delivery applications. Note that the release kinetics is closely linked to the droplet size. Multiple microfluidic geometries were attempted in the past to successfully produce monodisperse double emulsions. For example, Nisisako et al. [25] and Romanowsky et al. [26] used consecutive planar Tjunctions to form both O/W/O and W/O/W double emulsions, while Utada et al. [27] used co-axial glass capillaries in a flow-focussing setup to obtain O/W/O double emulsions, where the shell thickness varied in the range of 3-40% of the droplet radius. Chu et al. [28] extended the coaxial co-flow geometry to create additional hierarchical levels of emulsions, e.g., triple emulsions.

The strategies of obtaining double emulsions presented above can be extended to fabrication of core-shell microparticles, e.g., via solidification of the shell liquid after the double emulsion is obtained. One method uses a polymer solution in the organic shell liquid phase prior to double emulsion preparation. The evaporation of the organic solvent restores the solid polymer encapsulation [29]. This method finds application in protein encapsulation due to the ease of shell removal, thus facilitating protein release. Another method uses a monomer solution in the shell liquid – a

core-shell structure results after polymerization of the monomer [30]. Both photopolymerization and step-growth polymerization techniques are suitable for converting the monomeric liquid shell into a solid shell [31]. Although the present work is a ramification of the monomer polymerization technique, two primary distinctions of the present work are readily apparent. First, the shell materials are highly porous solids. Second, double emulsions from an oil-in-oil (O/O/O) emulsion system are easily produced via a strategic microfluidic delivery system.

The present work seeks to fabricate core-shell polyimide aerogel hollow microparticles using an O/O/O emulsion system. This in itself is a departure from typical microfluidic droplet generation schemes, where most microfluidic systems utilize a W/O or O/W system stabilized by surfactants [32]. While aerogels have been fabricated in a variety of structural forms such as monoliths [33]. foams [34,35] and microparticles [36,37], and even complex gyroid geometries [38], we believe that this work is the first to report core-shell aerogel microparticles with highly porous shell structures. Earlier studies [33-38] established that the polyimide precursor materials included in this work yield mesoporous gels. The polyimide gel microparticles in this work were supercritically dried to obtain core-shell aerogel microparticles with substantial mesopores. The first part of the work presents fabrication of gel microparticles without surfactants and shows that the flow rates and rheological properties of the shell liquid can be used to control size distribution of hollow microparticles. The second part assesses the effects of a block copolymer surfactant.

2. Experimental section

2.1. Materials

Pyromellitic dianhydride (PMDA) was purchased from Alfa-Aesar (Haverhill, MA) and 2,2'-dimethylbenzidine (DMBZ) was purchased from Shanghai Worldyang Chemical Co. Ltd (Shanghai, China). Tris(2-aminoethyl)amine (TREN) crosslinker and surfactant Pluronic® F127 were purchased from Sigma Aldrich (Milwaukee, WI). Pyridine, acetic anhydride, acetone, and silicone oil were purchased from Fisher Scientific (Ontario, NY). dimethylformamide (DMF) was purchased from VWR International (Radnor, PA) with a density of 0.944 g/cm³. A generic grade of silicone oil obtained from Fisher Scientific (Ontario, NY) with a density of 0.963 g/cm³ was used. The components of the droplet generator, such as 27 G and 20 G needles, 0.16 cm ID Tee connectors, Tygon® tubing and two-part epoxy were obtained from McMaster-Carr (Aurora, OH).

2.2. Fabrication of droplet generator

The co-flow double emulsion droplet generator used in this work was adapted from the work of Li et al.[39] This droplet generator was assembled by combining two co-flow droplet generators in sequence. The first co-flow droplet generator was assembled by connecting a 27 G flat tip needle to a 1.6 mm ID Tee connector using a 1.6 mm ID Tygon® tubing. Subsequently, a 20 G needle was attached to the other end of this first Tee connector. A second Tee connector was attached to the other end of the 20 G needle, Fig. 1a shows the unassembled components and Fig. 1b shows the components in their assembled state. All connection points were sealed with two-part epoxy sealant to prevent leakage. Fig. 1c shows schematically how the double emulsion was generated in this setup. In Fig. 1c, the inner liquid (silicone oil, viscosity ≈48.6 mPa·s) was introduced on the left through the 27 G needle. The inner liquid exits the 27 G needle and contacts the shell liquid (polyimide sol in DMF, viscosity ≈1.98 mPa·s). Rayleigh-Plateau

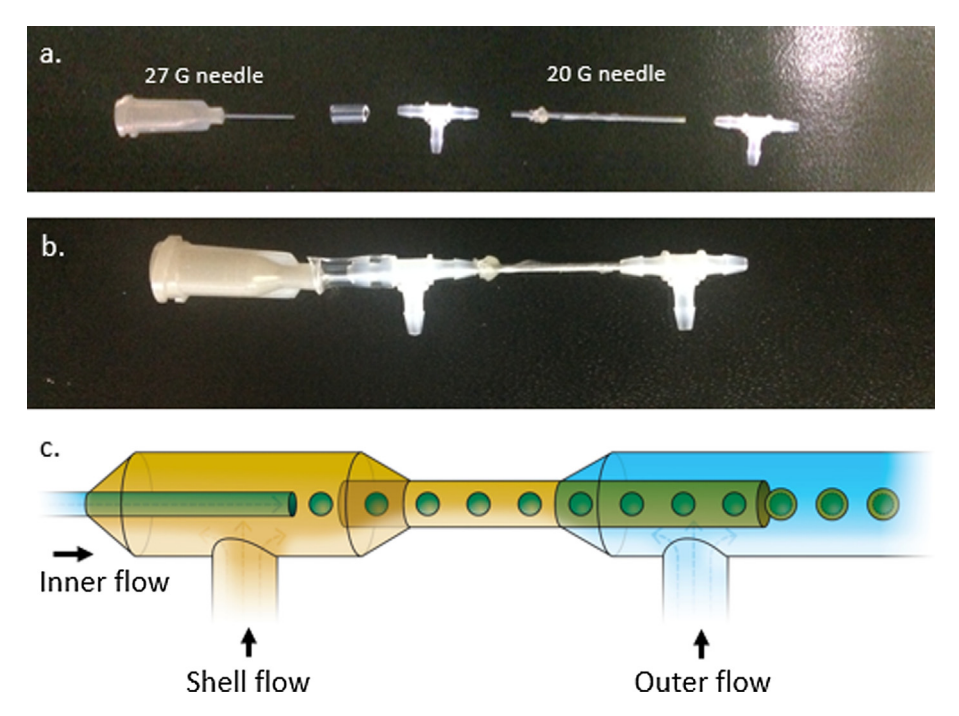


Fig. 1. Droplet generator components (a) before and (b) after assembly. (c) Schematic of double emulsion formation in droplet generator.

instability occurred on the silicone oil jet, transforming it to discrete droplets suspended in polyimide sol in DMF. The silicone oil droplets were then transferred downstream through the 20 G needle sheathed in the shell liquid of polyimide sol in DMF. The second emulsion was formed via the same mechanism as in the first emulsion, thus encapsulating the silicone oil droplets formed in the first Tee connector, with a shell liquid, i.e., polyimide sol in DMF. The second set of droplets were formed in silicone oil introduced in the second Tee connector. The shell liquid (polyimide sol in DMF) is immiscible with silicone oil. Thus, the shell liquid served as a barrier against coalescence of silicone oil confined in the core with silicone oil carrying the core-shell droplets. In this study, while we acknowledge that no two liquids are completely immiscible, we have treated the silicone oil/DMF system as one with very low mutual solubility. These two liquids, upon contact, form two distinct phases.

Fig. 2 presents a sequence of images taken at various elapsed times to show the formation of double emulsion at the tip of the second Tee connector. The starting point is the image of an inner liquid droplet encapsulated within the jet of the shell liquid at the tip of the second Tee connector (Fig. 2a and g). As the liquid jet comes out of the tip of the second Tee connector, capillary pressure is exerted on the growing jet, leading to detachment of a dro-

plet from the jet tip. The sequence of droplet formation captured in Fig. 2 indicates that droplet formation was governed by the jetting regime; droplet detachment occurred downstream from the outlet orifice of the second Tee connector, as illustrated using sketches in Fig. 2(h–l) [40]. For double emulsion formation, the inner flow rate $(Q_{\rm in})$ of silicone oil was maintained at 0.08 mL/min, the shell flow rate $(Q_{\rm shell})$ of polyimide sol in DMF was varied in the range of 0.2–0.5 mL/min, and the outer flow rate $(Q_{\rm out})$ of silicone oil was varied from 1 to 4 mL/min.

2.3. Preparation of shell liquid

In the first part of the paper, hollow microparticles were fabricated without a surfactant, while in the second part, the effects of surfactant addition were evaluated. In the first part, the shell liquid of polyimide precursor solutions (henceforth sol) was prepared at room temperature by mixing PMDA, DMBZ, and TREN in DMF, as per the process outlined by Teo and Jana [37]. Briefly, PMDA and DMBZ, dissolved separately in DMF, were mixed with a magnetic stirrer at 1000 rpm for 2 min at room temperature. Subsequently, TREN, acetic anhydride, and pyridine were added to trigger crosslinking reactions and to allow chemical imidization of the polyamic acid. The solution was magnetically stirred for an

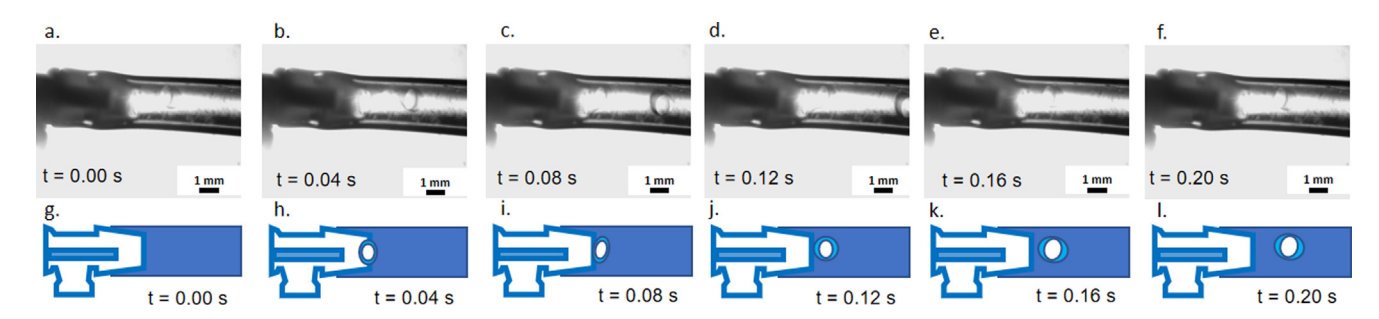


Fig. 2. (a-f) High speed camera images of second emulsion formation at the end of the second Tee connector. (g-l) correspond to schematics of droplet detachment from the jet, highlighting approximate droplet locations.

additional 1.5 min. A typical polyimide sol sample with 3.9 wt% polymer concentration was prepared using 0.108 g PMDA, 0.106 g DMBZ, 10 μ L TREN, 0.333 g acetic anhydride, 0.313 g pyridine, and 5.0 mL of DMF. A higher than stoichiometric amount of TREN crosslinker was used to obtain appropriate gelation times [37,41]. After stirring all the ingredients for 1.5 min, the polyimide sol was immediately transferred into a syringe pump for injection into the droplet generator.

For the second part, a measured amount of Pluronic® F127 surfactant, a PEO-PPO-PEO triblock copolymer was added to the solution of PMDA. The rest of the sol preparation process was identical to the first part.

2.4. Fabrication of polyimide aerogel core-shell hollow microparticles

The fabrication of core-shell microparticles mirrors closely the fabrication process outlined by Teo and Jana [37] for fabrication of aerogel microparticles. The inner liquid (silicone oil) was injected into the droplet generator directly through the 27 G needle via a syringe. The shell liquid (polyimide sol in DMF) and outer liquid (silicone oil) were introduced into droplet generators via Tygon® tubing, following the schematic presented in Fig. 1. All liquid flows were delivered through Chemyx syringe pumps (Stafford, TX). The generated double emulsion droplets were guided into a heated silicone oil bath for gelation and subsequent collection.

The silicone oil bath was kept at a temperature of 80 °C to enable fast gelation of the polyimide sol shell liquid. After gelation, the core-shell gel microparticles were aged further in silicone oil for 24 h, subsequently removed from silicone oil, and washed with chloroform. The gel microparticles were subsequently solvent exchanged sequentially with mixed solvents consisting of 25 vol % acetone/75 vol% chloroform, 50 vol% acetone/50 vol% chloroform, 75 vol% acetone/25 vol% chloroform, and finally with 100 vol% acetone each at 12 h intervals. In addition, the gel microparticles were further washed with 100 vol% acetone for an additional 5 times at 12 h intervals to remove traces of DMF, silicone oil, and chloroform from the gels. The gels were subsequently solvent exchanged with liquid carbon dioxide in an autoclave by washing with 100 vol% liquid carbon dioxide for 6 times at 1.5 h intervals. The liquid carbon dioxide filled gels were subsequently dried under supercritical condition of carbon dioxide at 50 °C and 11 MPa pressure to yield aerogel microparticles.

2.5. Characterization of aerogel core-shell microparticles

2.5.1. Gel and aerogel core-shell microparticle size distribution

The size distributions of gel and aerogel microparticles were studied using an Olympus BX51 optical microscope (OM). The images of a population of microparticles were collected and analyzed using the ImageJ software. Typically, the sizes of more than 100 microparticles were considered in each case. For each set of microparticles, the *outer diameter* and the diameter of the hollow core, henceforth termed as *inner diameter* were recorded. The shell thickness was calculated from the difference of outer diameter and inner diameter values of hollow microparticles measured from optical microscope images. We note that the density difference between the shell (polyimide sol in DMF) and core (silicone oil) liquids caused the core liquid to move off-centered before gelation of the shell liquid. This was more apparent for microparticles with thicker shells.

2.5.2. Aerogel morphology

The morphology of aerogels was studied using a scanning electron microscope (SEM, JSM5310, JEOL, MA) at an accelerating voltage of 2 kV and emission current of 20 mA. A representative piece of fractured aerogel specimen was mounted on an aluminum stub

using carbon tape, followed by sputter coating with silver (ISI-5400 Sputter Coater, Polaron, UK).

IR: Infrared spectra were collected on a Nicolet iS50 FTIR tridetector spectrophotometer (Thermo Scientific, MA).

2.5.3. Interfacial tension measurements

The interfacial tension between DMF and silicone oil was measured using a Du Noy tensiometer (Interfacial Tensiometer 70545, Central Scientific Co., VA) as function of Pluronic® F127 concentration. Data were taken in triplicate.

2.5.4. TGA

Thermogravimetric analysis (TGA) was conducted under N_2 environment with a Q50 thermogravimetric analyzer (TA Instruments, DE) using a heating rate of 20 °C/min, up to 800 °C.

2.5.5. Brunauer-Emmett-Teller (BET) surface area

BET surface area and pore size distribution of aerogel specimens were obtained from N_2 adsorption-desorption isotherms at 77 K, using a Micromeritics Tristar II 3020 analyzer (Micromeritics Instrument Corp. GA).

3. Results and discussion

3.1. Morphology of gel and aerogel hollow microparticles without surfactant

The process described in the experimental section allowed successful formation of discrete core-shell aerogel microparticles. In the first part of the study, no surfactant was used. Representative OM and SEM images of gel and deliberately fractured aerogel microparticles are shown in Fig. 3. The images in Fig. 3(b–e) were obtained by sputter coating a collection of deliberately fractured core-shell microparticles. These images revealed the internal structures and porous shell of the core-shell particles.

The optical images in Fig. 3a show that the gel droplets were spherical and of diameter close to 700 μm . The amber yellow color is a signature of polyimide gel. The SEM image in Fig. 3b shows the surfaces and a thin shell of a broken, hollow microparticle. The inside and outside surfaces of the microparticle appear smooth on a scale of 100 µm. The shell with a thickness of less than 10 µm is highlighted in Fig. 3c. The SEM images in Fig. 3d and e show high magnification images of the outer and inner surfaces of the hollow microparticles. Both these images show that the inner and outer surfaces of the shell were porous aerogel structures composed of fibrillar polyimide strands of typical diameter 12.9 ± 2.3 nm. It is apparent from Fig. 3d and e that the inner and outer surfaces of the polyimide shell had similar morphology, which is not surprising in view of the same two liquids, polyimide sol in DMF and silicone oil formed the two interfaces. The high magnification image in Fig. 3f show porous structures in the polyimide shell.

3.2. Microparticle size distribution

The diameter distribution of microparticles was studied as functions of both the shell and outer flow rates. The inner flow rate was kept constant at 0.08 mL/min for all experiments. Fig. 4 and Table 1 show microparticle size distributions and the average diameter of both gels and aerogel microparticles fabricated without surfactant.

An increase of the outer flow rate (Q_{out}) from 1.0 to 4.0 mL/min led to reduction of average gel and aerogel microparticle diameter from 845 to 774 μm and from 823 to 778 μm respectively (Table 1). The microparticle size distributions also narrowed as shown in

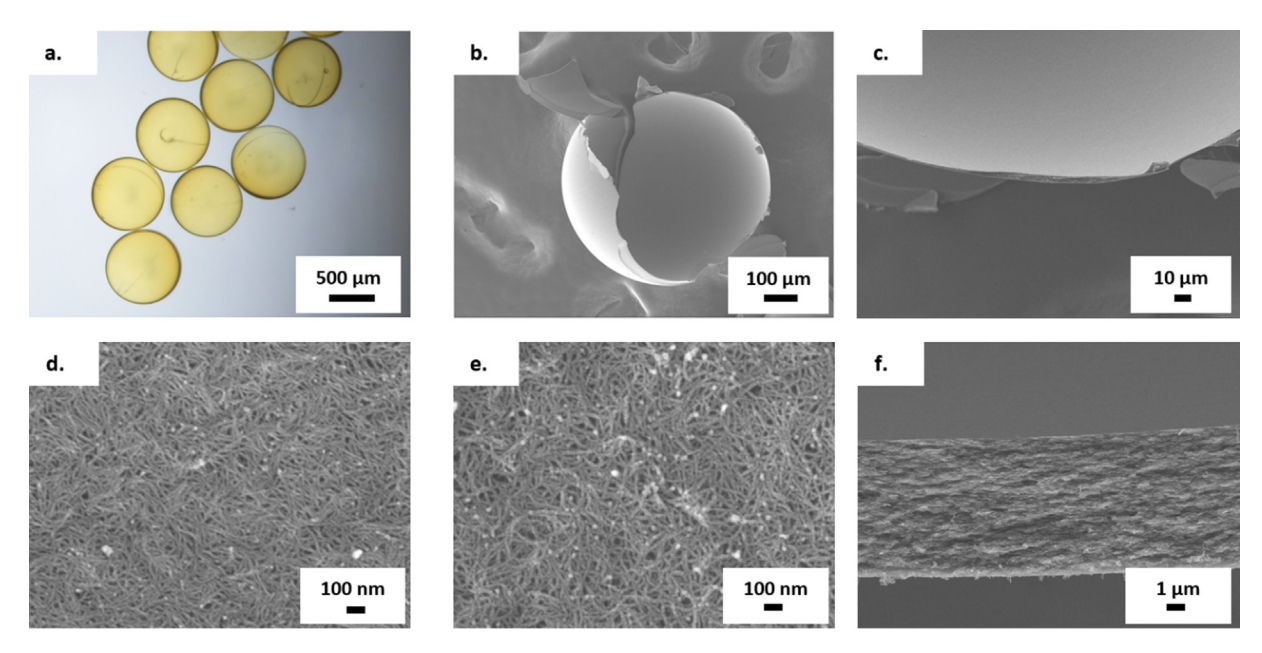


Fig. 3. Representative images of microparticles. (a) Optical image of gel microparticles. (b–e) SEM images of deliberately fractured core-shell microparticles. (b) Core-shell nature of microparticles, (c) shell, (d) porous morphology of outer surface of the shell, (e) porous morphology of the inner surface of the shell, and(f) porous morphology of the cross-section of the shell. The core-shell microparticles were produced with $Q_{in} = 0.08 \text{ mL/min}$, $Q_{shell} = 0.2 \text{ mL/min}$ and $Q_{out} = 4.0 \text{ mL/min}$.

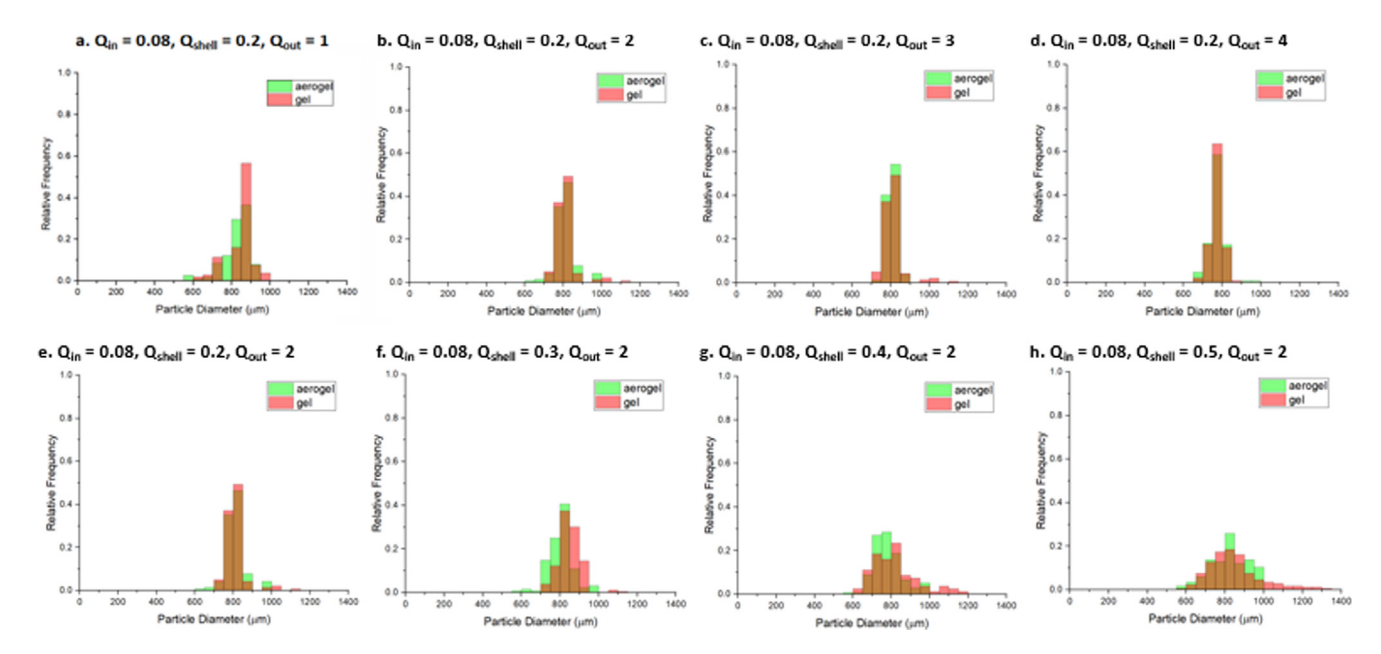


Fig. 4. Gel and aerogel microparticles outer diameter distributions for different flow rates. No surfactant was used. The set of numbers indicated above each graph represents the inner/shell/outer flow rates in mL/min. Red bars correspond to gel microparticles while green bars correspond to aerogel microparticles.

Table 1Average gel and aerogel microparticle outer diameter and shell thickness. No surfactant was used.

Inner Flow Rate – Q _{in} (mL/min)	Shell Flow Rate – Q _{shell} (mL/min)	Outer Flow Rate – Q _{out} (mL/min)	Average Gel Microparticle Diameter (μ m)	Average Aerogel Microparticle Diameter (µm)	Average Shell Thickness (μm)	Volume Shrinkage (%)
0.08	0.2	1.0	845 ± 72	823 ± 70	140	2.6
		2.0	812 ± 54	828 ± 82	84	- 2.0
		3.0	804 ± 24	808 ± 43	43	- 0.5
		4.0	774 ± 30	778 ± 52	22	- 0.5
	0.3	2.0	847 ± 58	830 ± 111	103	5.9
	0.4		789 ± 90	810 ± 118	170	2.7
	0.5		847 ± 137	833 ± 123	321	1.7

Fig. 4a–d. This reduction in gel and aerogel microparticle size with an increase of outer flow rate (Q_{out}) is due to higher viscous force. The liquid jet underwent strong elongation and produced smaller droplets after detaching from the jet tip. The data in Fig. 4a–d and Table 1 also show that the size distribution of microparticles narrowed substantially with an increase of outer flow rate (Q_{out}). The standard deviation of microparticle diameter reduced from 72 μm to 30 μm as the value of Q_{out} was increased from 1.0 to 4.0 mL/min. In this context, we note that a narrowing jet at higher value of Q_{out} is able to suppress the capillary instability, resulting in droplets with narrow size distribution.[42]

An increase of Q_{out} also led to lowering of shell thickness of the gel, e.g., 140 μm at Q_{out} of 1.0 mL/min to 22 μm at Q_{out} of 4.0 mL/min (Table 1). In this case, viscous force became stronger at higher values of Q_{out} , resulting in thinning of the shell liquid thread before droplet formation. The core liquid diameter, however, remained unchanged as the core droplet of silicone oil was generated upstream.

The average gel microparticle diameter remained relatively insensitive to an increase of Q_{shell}, but the size distribution broadened considerably, as seen in Fig. 4e-h. A high shell flow rate increases the velocity of the jet extruded from the second needle (20 G) into the outer flow. This shifts the droplet generation regime from jetting to a widening jet regime. In this case, the dispersed phase velocity is higher than the continuous phase velocity. This in turn leads to deceleration of the shell liquid as it exits the second needle, thereby causing a local buildup of the shell liquid in the thread, resulting in uneven droplet size. Another result of an increase of Q_{shell} is higher shell thickness, e.g., 84 μm for Q_{shell} of 0.2 mL/min to 321 μm for Q_{shell} of 0.5 mL/min for the same Q_{out} of 2.0 mL/min (Table 1). An increase of shell thickness is evident from the SEM images of a collection of deliberately fractured core-shell microparticles presented in Fig. 5(a-d). SEM images of representative whole core-shell aerogel microparticles are shown in Fig. 5(e-h). The porous nature of polyimide shells are evident from the SEM images presented in Fig. 5(i-l).

The overlapping diameter distributions of gel and aerogel microparticles in Fig. 4 also indicates negligible shrinkage of the gels upon supercritical drying. This low shrinkage is to be expected as shrinkage comes from the gel component of the hollow microparticles, which in this case only accounted for a thin shell section that is less than 10% of the total diameter of the microparticle. The negative values of shrinkage reported in Table 1 do not indicate that the aerogels expanded upon supercritical drying, but rather an artifact of shifting of the mean size in population of gel and corresponding aerogel microparticles.

3.3. Effect of surfactant

The results presented in previous section established that coreshell gel and aerogel microparticles can be produced from silicone oil/DMF/silicone oil (O/O/O system) without the addition of a surfactant. The gel microparticle droplets, generated in the droplet generator (Fig. 1), were guided into hot silicone oil to obtain gelation of the shell liquid within ~10 s [37]. This eliminated the possibility of droplet coalescence. One may wonder if the addition of a surfactant would exert any effects on size of the microparticles and the shell liquid thickness. Teo and Jana [41] showed earlier that the addition of a PEO-PPO-PEO triblock copolymer surfactant, Pluronic® F127 modified the morphology of polyimide aerogel. Specifically, the addition of Pluronic®F127 surfactant helped increase the diameter of polyimide strands in the aerogel.

We note here that the addition of Pluronic[®] F127 lowered the interfacial tension between silicone oil and DMF from a value of 4.0 mN/m with no surfactant to 1.8 mN/m in the presence of 1.0 vol% of Pluronic[®] F127 in DMF. Note that PEO-PPO-PEO block copolymer is a known surfactant for oil-in-oil (O/O) emulsion systems.[43,44] The presence of Pluronic[®] F127 at 2.5 and 5.0 vol%

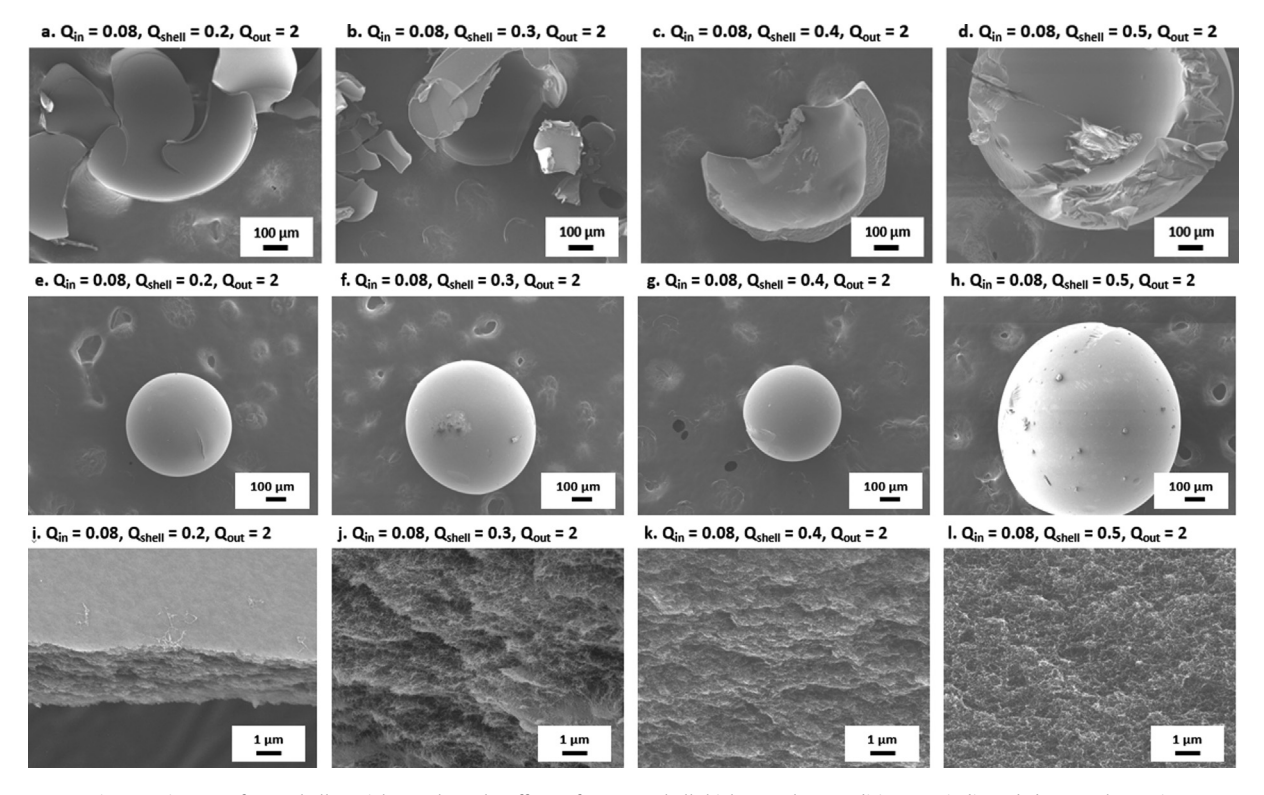


Fig. 5. Representative SEM images of core-shell particles to show the effects of Q_{shell} on shell thickness. Flow conditions are indicated above each SEM image. Images in (a)–(d) show the shells of deliberately fractured core-shell particles at $100 \times$ magnification, (e)–(h) show the whole core-shell particles at $65 \times$ magnification, while (i)–(l) show the shell walls of the respective particles at $10,000 \times$ magnification, highlighting the porous nature of the shell.

had marginal effect on the interfacial tension, e.g., 1.7 mN/m and 1.6 mN/m respectively indicating that critical micelle concentration of Pluronic®F127 in DMF and silicone oil system was less than 1.0 vol%, in line with other studies of Pluronic® block copolymers in aqueous systems.[45] Our earlier work [41] established that the addition of Pluronic® F127 also increases the viscosity of polyimide sol in DMF. In this part of the paper, the effects of reduction of interfacial tension and an increase of viscosity of polyimide sol on microparticle size distributions are discussed. At this point, it is also worthwhile to note that characterization of emulsion of a DMF/silicone oil/F127® system was not studied as no bulk emulsion was created in this work. The purpose of adding F127® was not to promote its role as a surfactant in forming emulsions, but as a rheological modifier and to tune the interfacial tension values. We contend that emulsion droplets in this work were formed in a controlled and sequential manner and not through a bulk method such as stirring or other large-scale agitation. As a result, the values of flowrates, surface tension, and viscosity at the jet tip were critical in determining the size of individual droplets.

The data presented in Fig. 6 and Table 2 show that the addition of Pluronic® F127 had distinct influence on the size distribution of microparticles, for the same set of flow rates of the core, shell, and outer liquids. Two different trends are observed with an increase of Pluronic®F127 concentration. First, the microparticle size distribution shifted to larger diameter. This can be seen in Table 2. The average gel microparticle diameter increased from 659 \pm 28 μm to 832 \pm 52 μm as the concentration of Pluronic® F127 was increased from 0.0 to 5.0 vol%. Second, the size distribution became wider in the presence of Pluronic® F127, as evident from Fig. 6 and the standard deviation values of the gel microparticles reported in Table 2. These trends are also reflected in the size distributions of aerogel microparticles.

The shell thickness also shifted to higher values in the presence of Pluronic® F127. Fig. 7 shows the shell thickness distribution of hollow microparticles fabricated with varying concentrations of Pluronic®F127. The shell thickness of gel microparticles in this case was obtained from the difference of outer diameter of the microparticle and the diameter of the core liquid of the same microparticle inferred from optical images. The data in Fig. 7a–d indicate that the shell thickness increased and the shell thickness distribution broadened with an increase of Pluronic®F127 concentration. This increase in shell thickness is visually inferred from the representative SEM images shown in Fig. 7e–h. We note here that the diameter of the core liquid (silicone oil) showed weak dependence on the concentrations of Pluronic®F127, as reflected from the data presented in Fig. 7i–l.

We now refer to the mechanism of droplet formation in order to understand the effect of Pluronic®F127 concentration on diameter distribution and shell thickness of the microparticles. Recall that droplet formation in this system occurred via a jetting regime. In

Table 2Average gel and aerogel hollow microparticle diameter as function of surfactant concentration.

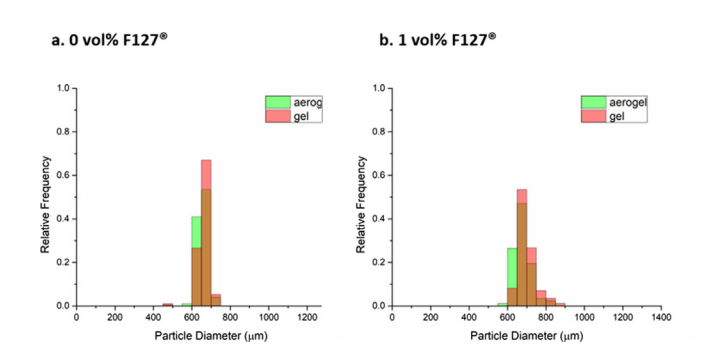
Pluronic® F127 concentration (vol%)	Average gel microparticle diameter (µm)	Average aerogel microparticle diameter (µm)	Volume shrinkage (%)
0.0	659 ± 28	655 ± 28	0.6
1.0	702 ± 44	678 ± 44	5.3
2.5	757 ± 30	744 ± 31	1.7
5.0	832 ± 52	776 ± 40	6.7

this regime, a liquid jet is first extruded from the tip of the inner orifice of the co-flow setup. The liquid jet experiences Rayleigh-Plateau instability and a major part of the extended liquid jet detaches to form a droplet. In this context, the interfacial force between the two liquid phases needs to overcome the viscous and inertial force of the extruded jet to break off the liquid from the jet and subsequently form a droplet. As alluded to earlier, the addition of Pluronic® F127 causes an increase of the viscous force of the shell liquid and reduction of interfacial tension between the liquid phases. These, in combination, delay droplet formation. Thus, at higher Pluronic®F127 concentration, a longer liquid jet is extruded and a bigger droplet is formed to accommodate higher volume of the liquid in the extended jet. The effects of changes in viscosity and interfacial tension on droplet formation are seen from the sequences of high-speed camera images presented in Fig. 8. The droplet detachment for both 0.0 and 5.0 vol% Pluronic® F127 systems was found to occur at 0.06 s. In Fig. 8j, the double emulsion droplet detaches at 2.8 mm away from the 20 G syringe tip, indicating a longer jet for the 5.0 vol% F127® system and hence bigger droplets in this case. For the system with no surfactant, the double emulsion droplet detaches at about 2.0 mm from the 20 G syringe tip (Fig. 8d).

An increase of the viscous force of the extruded jet also magnifies the droplet breakoff instability, resulting in non-uniform droplet sizes and polydispersity in the gel microparticle diameter and shell thickness seen in Figs. 6 and 7 respectively.

The addition of Pluronic® F127 also changed the nanoscale morphology of the polyimide strands in the resultant polyimide aerogel. Fig. 9 shows the cross-sectional SEM images of the polyimide aerogel microparticles prepared with various Pluronic®F127 concentration. The strand diameter increased from 9.2 \pm 2.1 nm to 11.8 \pm 2.6 nm as the Pluronic®F127 concentration was increased from 0 to 5.0 vol%. The increase in strand diameter can be attributed to higher viscosity of the polyimide sol, thus allowing longer times for phase separation and coarsening of polymer strands during sol-gel transition.[41]

The increase of polyimide strand diameter also influenced the BET surface area values. The BET surface area values reduced from 179 m^2/g with no surfactant to 152, 79, and finally 50 m^2/g for



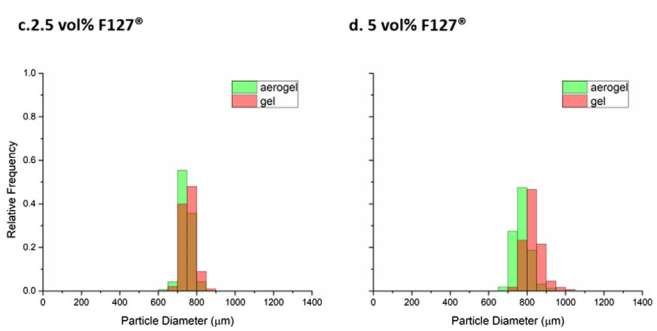


Fig. 6. Gel and aerogel hollow microparticles size distributions for different F127 $^{\circ}$ concentrations, (a) 0.0, (b) 1.0, (c) 2.5, and (d) 5.0 vol%. Flow conditions were kept the same: $Q_{in} = 0.08$ mL/min, $Q_{shell} = 0.2$ mL/min and $Q_{out} = 5.0$ mL/min.

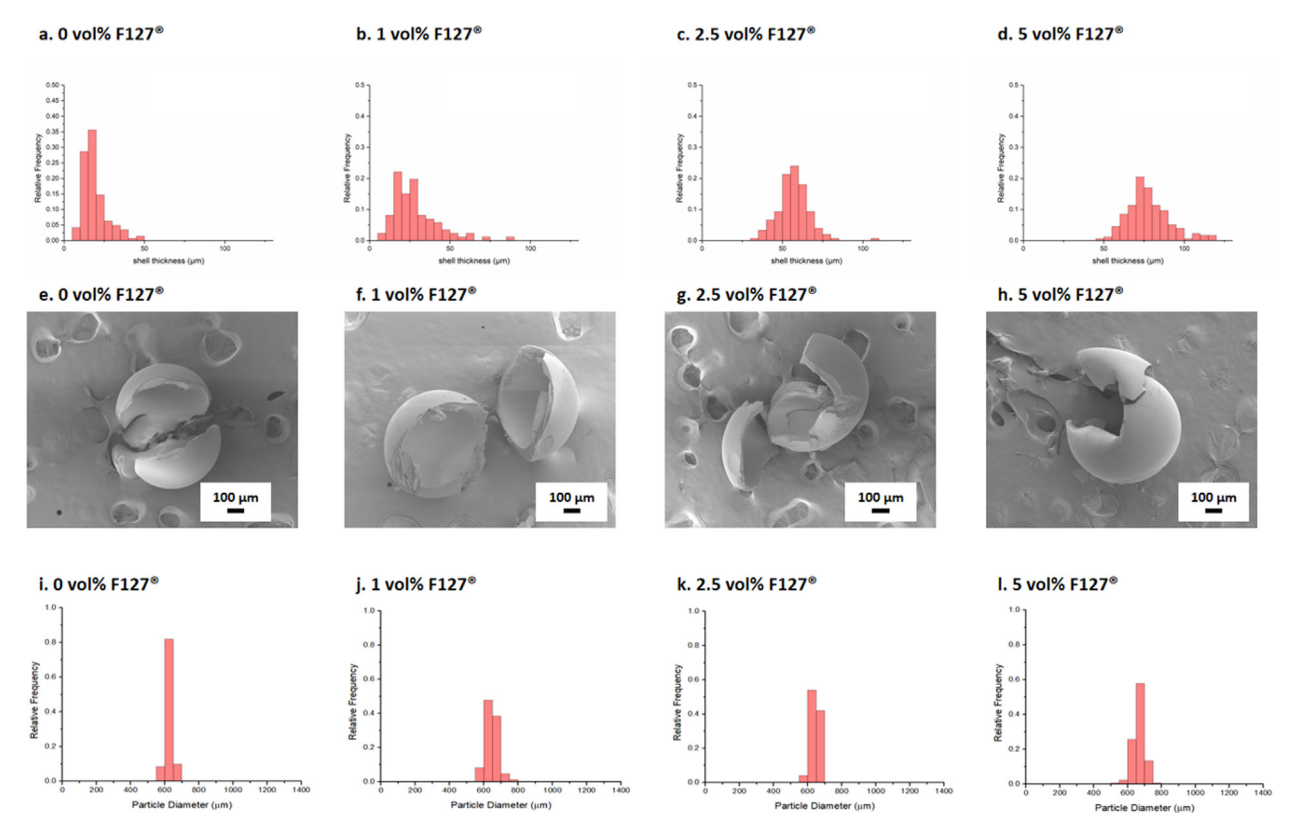


Fig. 7. Shell thickness distribution of hollow microparticle with (a) 0.0, (b) 1.0, (c) 2.5, and (d) 5.0 vol% F127®. Representative fractured hollow microparticles prepared with (e) 0.0, (f) 1.0, (g) 2.5, and (h) 5.0 vol% Pluronic®F127.Inside diameter of hollow microparticles prepared with(i) 0.0, (j) 1.0, (k) 2.5, and (l) 5.0 vol% Pluronic®F127.

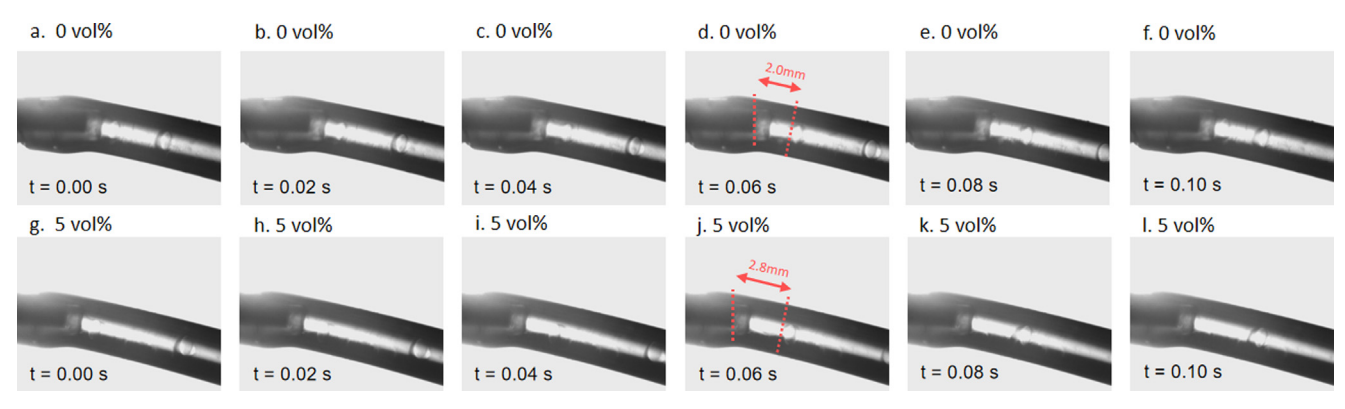


Fig. 8. Double emulsion droplet detachment from 20 G syringe tip for (a-f) 0 vol% and (g-l) 5 vol% Pluronic®F127. Droplet was seen to detach from jet in (d) and (j).

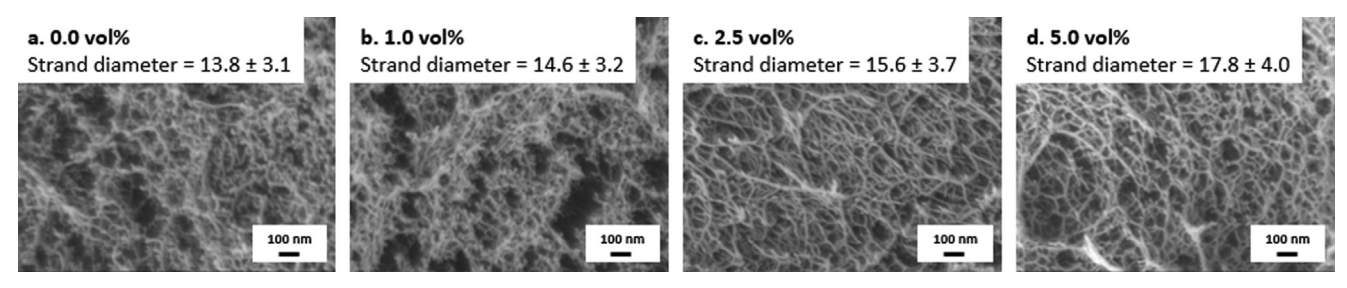


Fig. 9. SEM cross-sectional images of hollow microparticles with (a) 0, (b) 1, (c) 2.5, and (d) 5.0 vol% Pluronic® F127.

Pluronic®F127 concentration of 1.0, 2.5, and 5.0 vol% respectively. We note that thicker strands present lower surface area for the same skeletal density. The aerogel microparticles prepared using

the surfactant also had smaller fractions of mesopores as evident from the smaller area under the hysteresis loops in BET isotherms shown in Fig. 10a.

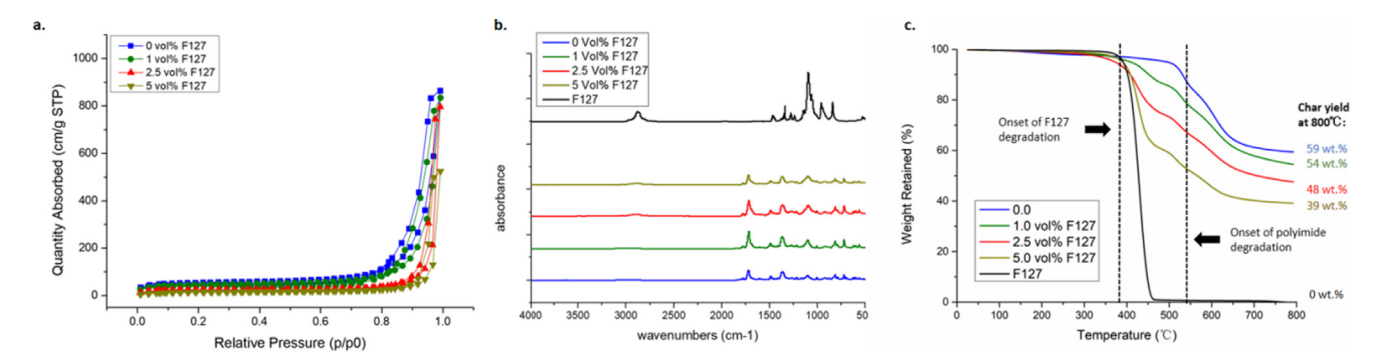


Fig. 10. (a) BET isotherm, (b) IR spectra, and (c) TGA traces of hollow microparticles with various Pluronic®F127 concentrations.

The data presented in Fig. 10b show the IR spectra of polyimide hollow aerogel microparticles with and without Pluronic®F127. The blue spectrum in Fig. 10b corresponding to aerogels with no surfactant indicate that the imide functional groups were successfully formed through chemical imidization. The absorbance bands at 1716 and 1776 cm⁻¹, corresponding to the symmetrical and asymmetrical stretching of the C=O group and the band at 1365 cm⁻¹, associated with the C—N stretching indicate the presence of imide rings in the structure. The absence of absorbance peaks due to COOH (2926 cm⁻¹) and CONH (3273 cm⁻¹) bands confirm imidization of polyamic acid. In reference to the spectrum of neat Pluronic®F127 (black spectrum) in Fig. 10b, we infer that aerogel microparticles prepared with Pluronic®F127 retained traces of the surfactant in the structures despite repeated washing with solvents. The absorbance bands at 2880 cm⁻¹ and 1100 cm⁻¹ corresponding to the alkane and ether groups respectively of the PEO-PPO-PEO structure of Pluronics® F127 appeared in such aerogel specimens. The C—O—C peak of Pluronic®F127 and imide ring deformation band both overlapped at 1100 cm⁻¹.

This residual amounts of Pluronic®F127 in the aerogel structures are also inferred from the TGA traces presented in Fig. 10c. It is noted that degradation of Pluronic®F127 surfactant started at around 350 °C (5% weight loss at 393 °C) with no char residue at 800 °C. In contrast, neat PI aerogels started degrading at 443 °C (5% weight loss) and had a char yield of 59 wt%. The char yield from hollow microparticles at 800 °C varied with Pluronic®F127 concentration used in the synthesis step. The char yield reduced with an increase of Pluronic®F127 concentration, e.g., 54, 48, and 39 wt% for Pluronic®F127 concentrations of 1.0, 2.5, and 5.0 vol% respectively. The above data indicate that the hollow aerogel microparticles contained residual Pluronic®F127 despite repeated washing during the solvent exchange step.

4. Conclusion

The results presented in this paper established the utility of a microfluidic flow system in fabrication of hollow core-shell polyimide aerogel microparticles via an oil-in-oil-in-oil emulsion system. A rapid sol-gel transition of the shell liquid promoted by a high temperature oil bath prevented droplet coalescence. The results show that the use of surfactants is optional in fabrication of hollow, core-shell aerogel microparticles. The diameter of core-shell microparticles and the shell thickness show strong dependence on the ratio of the core and shell flow rates and the shear rate in the microfluidic setup. The presence of Pluronic®F127 surfactant in polyimide sol increases its viscosity and reduces interfacial tension with silicone oil. These factors delay droplet breakoff from extended liquid jets thus yielding larger microparticles. The surfactant also reduces the mesopore volume due to thickening of polymer strands. This paper presents several tools

for design of core-shell aerogel microparticles of desired diameter, overall porosity, shell thickness, and mean pore size. We recognize that the core-shell aerogel microparticles produced in this research are of relatively large size and of wide size distribution. As discussed earlier, the purpose was to showcase continuous fabrication of these novel core-shell aerogel microparticles using a microfluidic flow system assembled from relatively cheap materials. Our future work will focus on obtaining much smaller core-shell aerogel microparticles with much narrower size distribution using commercially available microfluidic chips and associated pump systems.

CRediT authorship contribution statement

Nicholas Teo: Conceptualization, Methodology, Data curation, Validation, Formal analysis, Writing-original draft, Writing – review & editing. Chenxi Jin: Methodology, Formal analysis, Validation; Writing – review & editing. Akshata Kulkarni: Methodology, Formal analysis, Validation; Writing – review & editing. Sadhan C. Jana: Conceptualization, Investigation, Funding acquisition, Project administration, Supervision, Writing – review & editing.

Declaration of Competing Interest

The authors declared that there is no conflict of interest.

Acknowledgement

This work is partially funded by United States National Science Foundation under grant number CMMI 1826030.

References

- C.P. Champagne, P. Fustier, Microencapsulation for the improved delivery of bioactive compounds into foods, Curr. Opin. Biotechnol. 18 (2) (2007) 184– 190, https://doi.org/10.1016/j.copbio.2007.03.001.
- [2] L. Jackson, K. Lee, Microencapsulation and the food industry, LWT Food Sci. Technol. 24 (1991) 289–297.
- [3] S. Benita, Microencapsulation: Methods and Industrial Applications, second ed., CRC Press, 2005.
- [4] I.M. Martins, M.F. Barreiro, M. Coelho, A.E. Rodrigues, Microencapsulation of essential oils with biodegradable polymeric carriers for cosmetic applications, Chem. Eng. J. 245 (2014) 191–200, https://doi.org/10.1016/j.cej.2014.02.024.
- [5] R. Tekin, N. Bac, H. Erdogmus, Microencapsulation of fragrance and natural volatile oils for application in cosmetics, and household cleaning products, Macromol. Symp. 333 (1) (2013) 35–40, https://doi.org/ 10.1002/masy.201300047.
- [6] S. Higashi, T. Setoguchi, Hepatic arterial injection chemotherapy for hepatocellular carcinoma with epirubicin aqueous solution as numerous vesicles in iodinated poppy-seed oil microdroplets: clinical application of water-in-oil-in-water emulsion prepared using a membrane emulsification technique, Adv. Drug Deliv. Rev. 45 (1) (2000) 57–64, https://doi.org/10.1016/ S0169-409X(00)00100-9.

- [7] M.N. Singh, K.S.Y. Hemant, M. Ram, H.G. Shivakumar, Microencapsulation: a promising technique for controlled drug delivery, Res. Pharm. Sci. 5 (2) (2010) 65–77
- [8] A. Gharsallaoui, G. Roudaut, O. Chambin, A. Voilley, R. Saurel, Applications of spray-drying in microencapsulation of food ingredients: an overview, Food Res. Int. 40 (9) (2007) 1107–1121, https://doi.org/10.1016/ j.foodres.2007.07.004.
- [9] M. Zhao, N.S. Zacharia, Protein encapsulation via polyelectrolyte complex coacervation: protection against protein denaturation, J. Chem. Phys. 149 (16) (2018) 163326, https://doi.org/10.1063/1.5040346.
- [10] M. Zhao, S.A. Eghtesadi, M.B. Dawadi, C. Wang, S. Huang, A.E. Seymore, B.D. Vogt, D.A. Modarelli, T. Liu, N.S. Zacharia, Partitioning of small molecules in hydrogen-bonding complex coacervates of poly(acrylic acid) and poly (ethylene glycol) or pluronic block copolymer, Macromolecules 50 (10) (2017) 3818–3830, https://doi.org/10.1021/acs.macromol.6b02815.
- [11] L.-Y. Chu, R. Xie, J.-H. Zhu, W.-M. Chen, T. Yamaguchi, S. Nakao, Study of SPG membrane emulsification processes for the preparation of monodisperse coreshell microcapsules, J. Colloid Interface Sci. 265 (1) (2003) 187–196, https://doi.org/10.1016/S0021-9797(03)00350-3.
- [12] S. Omi, K. Katami, A. Yamamoto, M. Iso, Synthesis of polymeric microparticles employing SPG emulsification technique, J. Appl. Polym. Sci. 51 (1) (1994) 1– 11, https://doi.org/10.1002/app.1994.070510101.
- [13] G. Ma, M. Nagai, S. Omi, Preparation of uniform poly(lactide) microparticles by employing the shirasu porous glass (SPG) emulsification technique, Colloids Surf. Physicochem. Eng. Asp. 153 (1) (1999) 383–394, https://doi.org/10.1016/ S0927-7757(98)00460-9.
- [14] W. Seifriz, Studies in emulsions. III-V, J. Phys. Chem. 29 (6) (1924) 738–749, https://doi.org/10.1021/j150252a009.
- [15] A.T. Florence, D. Whitehill, Some features of breakdown in water-in-oil-in-water multiple emulsions, J. Colloid Interface Sci. 79 (1) (1981) 243–256, https://doi.org/10.1016/0021-9797(81)90066-7.
- [16] K. Pays, J. Giermanska-Kahn, B. Pouligny, J. Bibette, F. Leal-Calderon, Coalescence in surfactant-stabilized double emulsions, Langmuir 17 (25) (2001) 7758–7769, https://doi.org/10.1021/la010735x.
- [17] B. Tal-Figiel, The formation of stable W/O, O/W, W/O/W cosmetic emulsions in an ultrasonic field, Chem. Eng. Res. Des. 85 (5) (2007) 730–734, https://doi.org/ 10.1205/cherd06199.
- [18] N. Garti, C. Bisperink, Double emulsions: progress and applications, Curr. Opin. Colloid Interface Sci. 3 (6) (1998) 657–667, https://doi.org/10.1016/S1359-0294(98)80096-4
- [19] M.-F. Ficheux, L. Bonakdar, F. Leal-Calderon, J. Bibette, Some stability criteria for double emulsions, Langmuir 14 (10) (1998) 2702–2706, https://doi.org/ 10.1021/la9712717
- [20] M. Kanouni, H.L. Rosano, N. Naouli, Preparation of a stable double emulsion (W1/O/W2): role of the interfacial films on the stability of the system, Adv. Colloid Interface Sci. 99 (3) (2002) 229–254, https://doi.org/10.1016/S0001-8686(02)00079-9.
- [21] R.K. Shah, H.C. Shum, A.C. Rowat, D. Lee, J.J. Agresti, A.S. Utada, L.-Y. Chu, J.-W. Kim, A. Fernandez-Nieves, C.J. Martinez, et al., Designer emulsions using microfluidics, Mater. Today 11 (4) (2008) 18–27, https://doi.org/10.1016/S1369-7021(08)70053-1.
- [22] S. Okushima, T. Nisisako, T. Torii, T. Higuchi, Controlled production of monodisperse double emulsions by two-step droplet breakup in microfluidic devices, Langmuir 20 (23) (2004) 9905–9908, https://doi.org/10.1021/ la0480336.
- [23] G.F. Christopher, S.L. Anna, Microfluidic methods for generating continuous droplet streams, J. Phys. Appl. Phys. 40 (19) (2007) R319, https://doi.org/ 10.1088/0022-3727/40/19/R01.
- [24] S.-H. Kim, J.-W. Kim, J.-C. Cho, D.A. Weitz, Double-emulsion drops with ultrathin shells for capsule templates, Lab Chip 11 (18) (2011) 3162–3166, https:// doi.org/10.1039/C1LC20434C.
- [25] T. Nisisako, T. Torii, T. Takahashi, Y. Takizawa, Synthesis of monodisperse bicolored Janus particles with electrical anisotropy using a microfluidic co-

- flow system, Adv. Mater. 18 (9) (2006) 1152-1156, https://doi.org/10.1002/adma.200502431.
- [26] M.B. Romanowsky, A.R. Abate, A. Rotem, C. Holtze, D.A. Weitz, High throughput production of single core double emulsions in a parallelized microfluidic device, Lab Chip 12 (4) (2012) 802–807, https://doi.org/10.1039/ C21C21033A
- [27] A.S. Utada, E. Lorenceau, D.R. Link, P.D. Kaplan, H.A. Stone, D.A. Weitz, Monodisperse double emulsions generated from a microcapillary device, Science 308 (5721) (2005) 537–541, https://doi.org/10.1126/science.1109164.
- [28] L.-Y. Chu, A.S. Utada, R.K. Shah, J.-W. Kim, D.A. Weitz, Controllable monodisperse multiple emulsions, Angew. Chem. 119 (47) (2007) 9128– 9132, https://doi.org/10.1002/ange.200701358.
- [29] M. Iqbal, N. Zafar, H. Fessi, A. Elaissari, Double emulsion solvent evaporation techniques used for drug encapsulation, Int. J. Pharm. 496 (2) (2015) 173–190, https://doi.org/10.1016/j.ijpharm.2015.10.057.
- [30] J.-W. Kim, A.S. Utada, A. Fernández-Nieves, Z. Hu, D.A. Weitz, Fabrication of monodisperse gel shells and functional microgels in microfluidic devices, Angew. Chem. 119 (11) (2007) 1851–1854, https://doi.org/10.1002/ ange.200604206.
- [31] Y. Hennequin, N. Pannacci, C.P. de Torres, G. Tetradis-Meris, S. Chapuliot, E. Bouchaud, P. Tabeling, Synthesizing microcapsules with controlled geometrical and mechanical properties with microfluidic double emulsion technology, Langmuir 25 (14) (2009) 7857–7861, https://doi.org/10.1021/1a9004449.
- [32] A. Quell, J. Elsing, W. Drenckhan, C. Stubenrauch, Monodisperse polystyrene foams via microfluidics – a novel templating route, Adv. Eng. Mater. 17 (5) (2015) 604–609, https://doi.org/10.1002/adem.201500040.
- [33] S.J. Kim, P. Raut, S.C. Jana, G. Chase, Electrostatically active polymer hybrid aerogels for airborne nanoparticle filtration, ACS Appl. Mater. Interfaces 9 (7) (2017) 6401–6410, https://doi.org/10.1021/acsami.6b14784.
- [34] N. Teo, S.C. Jana, Open cell aerogel foams via emulsion templating, Langmuir 33 (44) (2017) 12729–12738, https://doi.org/10.1021/acs.langmuir.7b03139.
- [35] N. Teo, Z. Gu, S.C. Jana, Polyimide-based aerogel foams, via emulsion-templating, Polymer 157 (2018) 95–102, https://doi.org/10.1016/j.polymer.2018.10.030.
- [36] S. Gu, S.C. Jana, Open cell aerogel foams with hierarchical pore structures, Polymer 125 (2017) 1–9, https://doi.org/10.1016/j.polymer.2017.07.085.
- [37] N. Teo, S.C. Jana, Surfactant-free process for the fabrication of polyimide aerogel microparticles, Langmuir (2019), https://doi.org/10.1021/acs. langmuir.8b03841.
- [38] N. Teo, P. Joo, E. Amis, S. Jana, Development of intricate aerogel articles using fused filament fabrication, Appl. Polym. Mater. (2019), https://doi.org/ 10.1039/C6LC00967K (published on 28 May 2019).
- [39] T. Li, L. Zhao, W. Liu, J. Xu, J. Wang, Simple and reusable off-the-shelf microfluidic devices for the versatile generation of droplets, Lab Chip 16 (24) (2016) 4718–4724, https://doi.org/10.1021/acsapm.9b00301.
- [40] P. Zhu, L. Wang, Passive and active droplet generation with microfluidics: a review, Lab Chip 17 (1) (2017) 34–75, https://doi.org/10.1039/C6LC01018K.
- [41] N. Teo, S.C. Jana, Solvent effects on tuning pore structures in polyimide aerogels, Langmuir 34 (29) (2018) 8581–8590, https://doi.org/10.1021/acs. langmuir.8b01513.
- [42] S.L. Anna, Droplets and bubbles in microfluidic devices, Annu. Rev. Fluid Mech. 48(1)(2016) 285–309, https://doi.org/10.1146/annurev-fluid-122414-034425.
- [43] J. Periard, A. Banderet, G. Riess, Emulsifying effect of block and graft copolymers — oil in oil emulsions, J. Polym. Sci. [B] 8 (2) (1970) 109–114, https://doi.org/10.1002/pol.1970.110080210.
- [44] M. Klapper, S. Nenov, R. Haschick, K. Müller, K. Müllen, Oil-in-oil emulsions: a unique tool for the formation of polymer nanoparticles, Acc. Chem. Res. 41 (9) (2008) 1190–1201, https://doi.org/10.1021/ar8001206.
- [45] E. Batrakova, S. Lee, S. Li, A. Venne, V. Alakhov, A. Kabanov, Fundamental relationships between the composition of pluronic block copolymers and their hypersensitization effect in MDR cancer cells, Pharm. Res. 16 (9) (1999) 1373– 1379, https://doi.org/10.1023/A:1018942823676.